Journal of
Synchrotron Radiation

ISSN 0909-0495

Received 28 March 2007
Accepted 4 June 2007

A novel facility using a Laue focusing monochromator for high-pressure diffraction at the SRS, Daresbury, UK

Alistair R. Lennie,* David Laundy, Mark A. Roberts and Graham Bushnell-Wye

Daresbury Laboratory, Warrington WA4 4AD, UK. E-mail: a.lennie@dl.ac.uk

A novel Laue focusing monochromator has been developed to provide intense X-radiation for high-pressure diffraction experiments. A beamline using this monochromator has been successfully developed on station 9.5 at the SRS, Daresbury Laboratory. Contributions to resolution from monochromator bandpass and divergence due to focusing have been quantified and are used to assess experimental diffraction data from diamond-anvil cells recorded using image plates with X-rays at ~30 keV. This optical and beamline design could be readily adapted to use X-rays from a bending magnet on a third-generation synchrotron source.

Keywords: monochromator; high pressure; diffraction; focusing; diamond anvil; X-ray.

1. Introduction

The development of high-pressure angle-dispersive X-ray diffraction at the Photon Factory (Shimomura *et al.*, 1992) introduced image plates for collecting complete Debye–Scherrer powder diffraction rings, which were then integrated to provide high signal-to-noise ratio data. This technique overcame problems arising from the small sample volume contained in the diamond-anvil cell (DAC), allowing exploitation of the advantages of angle-dispersive methods for high-pressure structural studies. As this technique has developed, requirements for higher flux for more demanding high-pressure experiments have been satisfied by exploiting highly collimated intense X-ray beams of third-generation synchrotron sources (Hemley *et al.*, 2005).

At the Daresbury Synchrotron Radiation Source (SRS), we were interested in increasing the X-ray flux for the high-pressure experiments regularly undertaken on station 9.1 at this facility (Nelmes *et al.*, 1992; McMahon, 2004). Station 9.1 is only 15 m from a 5 T superconducting wavelength shifter and there is therefore high X-ray flux at short wavelengths for these experiments. However, the diffracted intensity is low because the incident beam size, being reduced by slits, is small (less than 100 μm typically) and the beam suffers absorption in the diamond anvils and the sample. As a result, exposures can take several hours to achieve good statistical accuracy. There is no opportunity to increase the X-ray flux by moving the experiment closer to the source; the only method of increasing the incident X-ray flux is to improve the X-ray optics. This required finding a solution to the problem of increasing X-ray intensity in the wavelength range ~0.4 to 0.5 Å without significant loss of resolution.

Our solution to this problem was found in the development of a focusing monochromator using Laue geometry to provide the monochromatic beam at the desired wavelength. Here we describe the monochromator and the implementation of this device as the X-ray source on a new station dedicated to high-pressure studies. The focusing provides a 100-fold increase in flux over the existing facility at station 9.1 on the SRS, reducing measurement times from hours to minutes. This has opened up the possibility of studying new problems at high pressure on a second-generation synchrotron; increased flux allows measurement of weakly scattering materials, an increased pressure range of measurement, and high-throughput screening of organic and pharmaceutical phases crystallized under high pressure.

2. Experimental requirements

2.1. General scope and objectives

Station 9.1 has been used for high-pressure studies at the SRS because of its high flux at short wavelengths. The radiation source is a superconducting 5 T wavelength-shifter insertion device on the 2 GeV electron storage ring. Station 9.1 is situated towards the edge (32.5 mrad from the centre) of the horizontal radiation fan from the wavelength shifter and sees two overlapping tangent point sources with magnetic fields of about 4 T and 2.5 T. The radiation from these sources is broad band with significant X-ray flux extending above 40 keV. For the DAC experiments, monochromatic beam is selected by a water-cooled channel-cut silicon monochromator [(111) reflection] operating at an energy close to 27 keV. This monochromatic beam is then collimated with a sub-100 μm

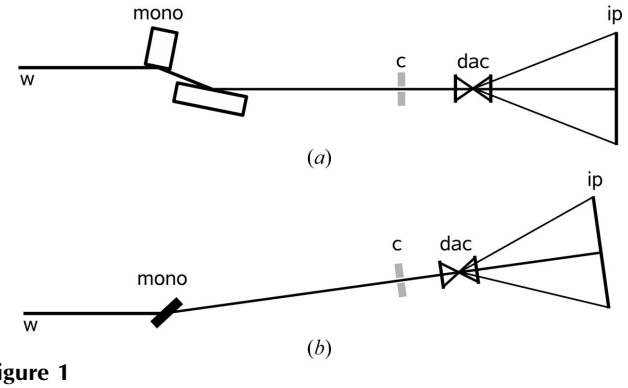

Figure 1
(*a*) Schematic layout of station 9.1 (side view). Monochromatic X-rays are selected from white radiation (w) by a double-bounce silicon monochromator (mono). The beam size is defined by a collimator/pinhole assembly (c) prior to entering the diamond-anvil cell (dac). X-rays are detected by an image plate (ip). (*b*) Schematic layout of station 9.5 (top view). White radiation (w) strikes the (100) face of a silicon crystal (mono), with vertical edges parallel to (110). The (111) reflection is selected by rotating to the Bragg angle (θ) required for a chosen energy. We use $\lambda = 0.44397$ Å (27.93 keV), calibrating on the In absorption edge. Bending the crystal focuses the monochromatic beam. The focused sideways-deflected monochromatic X-ray beam passes along an evacuated beam tube, and is defined by a pinhole/collimator assembly prior to entering the diamond-anvil cell (dac). An image plate (ip) records the diffraction pattern.

diameter pinhole before the DAC. A schematic diagram of the experimental set-up is shown in Fig. 1(*a*). At 27 keV, the calculated monochromatic X-ray flux passing through a 70 µm-diameter pinhole, for an electron beam current of 200 mA, is about 2×10^7 photons s^{-1}. An order of magnitude increase in this X-ray flux would be a major enhancement to the facility, reducing exposure times to below 1 h.

2.2. Requirements for the experiment

The optimum X-ray energy for the experiment is dependent on the requirement to obtain a sufficient number of Debye–Scherrer rings on the image-plate detector within the restricted angular range allowed by the DAC geometry while having sufficient resolution to separate rings closely spaced in *d*-space. In addition, the X-ray flux from the wiggler source falls off at high energies while at low X-ray energy the flux is reduced owing to absorption in both sample and diamond anvils. The presence of harmonic reflections from the monochromator may become a problem at lower X-ray energies. These considerations have led us to select an energy close to 30 keV which corresponds to a wavelength of $\sim$0.4 Å.

2.3. Contributions to experimental resolution

Experimental image-plate data consist of a series of concentric Debye–Scherrer rings. Intensity data are obtained by integrating around each ring at constant scattering angle 2θ to obtain the integrated scattered intensity at a lattice plane spacing distance $d = \lambda/[2\sin(\theta)]$. Instrumental broadening of the *d*-space resolution has an energy bandwidth (ΔE) and an angular resolution ($\Delta\varphi$) contribution and, in this experimental geometry, we can assume that these two contributions are uncorrelated. The energy bandwidth comes from the X-ray monochromator, and, for a perfect crystal silicon (111) monochromator such as that used on station 9.1, the contribution from the silicon intrinsic Darwin width to energy resolution is given by $\Delta E/E \simeq 10^{-4}$. In addition, the angular resolution has contributions from the divergence of the incident X-ray beam and the angular resolution of the detector. In the case of station 9.1, with no focusing optics, as the beam at the sample is very small, the incident-beam angular resolution depends on the size of the electron-beam X-ray source, approximately 0.45 mm high and 1.5 mm wide. At an experiment distance of $\sim$15 m from the source, this gives an angular resolution [full width at half-maximum (FWHM)] in the vertical diffraction plane of $\Delta\varphi \simeq 0.45 \times 10^{-3}/15 = 3 \times 10^{-5}$ and in the horizontal diffraction plane of $\Delta\varphi \simeq 1.5 \times 10^{-3}/15 = 10^{-4}$. The detector angular resolution is given in our experiment by the image-plate pixel size and the distance from the sample to the plate, and is typically of the order of 0.5×10^{-3}.

The width of the Debye–Scherrer ring on the image-plate detector is the result of the instrumental resolution broadening and the intrinsic sample line width. The sample-related resolution width is caused by size effects in the sample (the finite size of the diffracting crystallites) combined with the strain variation within or among the crystallites in the sample. These two effects vary with *d*-spacing in different ways which is the basis for separating the relative contributions by measuring several diffraction peaks at different *d*-values (Warren & Averbach, 1950). The detector resolution should ideally be an order of magnitude narrower than the total line width on the detector so that there are several points across the width of each diffraction peak in *d*-space allowing peak profile fitting to be performed.

In *d*-space, the contributions to resolution may be calculated using Bragg's law. The energy bandwidth contribution Δd_m is given by $\Delta d_m/d = \Delta E/E$ and the angular resolution contribution $\Delta d_{\rm div}$ is given by $\Delta d_{\rm div}/d = [(\Delta 2\theta)/2] \times [(2d/\lambda)^2 - 1]^{1/2}$ where $\Delta 2\theta$ is the spread in 2θ angle caused by the beam divergence and detector spatial resolution. The incident beam angle and reflected beam angle are related to the scattering angle 2θ and therefore we can write $\Delta 2\theta = \Delta\varphi$.

In designing new beamline optics, the effects of the optics on experimental resolution must be carefully considered. The principle behind the use of focusing is to collect a fan of X-rays and to deflect them into a small focal spot at the sample pinhole creating a higher X-ray flux density than in the unfocused beam. When focusing is employed, the X-ray beam divergence at the sample is no longer governed by the source size and the source-to-pinhole distance, as in the unfocused case, but by the size of the collected X-ray fan (Δx), and *D*, the distance between the focusing element and the pinhole ($\Delta\varphi = \Delta x/D$).

Focusing can be implemented in vertical or horizontal directions and degrades the diffraction resolution in the corresponding diffraction plane. The monochromator also affects the X-ray flux. For a broad-band X-ray source the monochromatic X-ray flux is proportional to the monochromator integrated reflectivity; therefore a wider bandpass gives higher X-ray flux (if the peak reflectivity is unchanged).

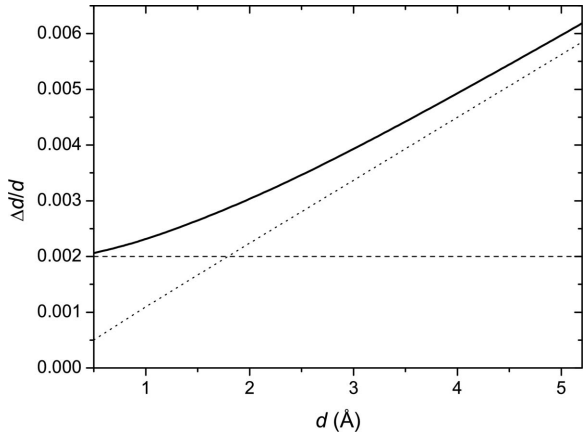

Figure 2
Instrumental resolution for the Laue monochromator at 30 keV. Energy bandwidth contribution for $\Delta E/E = 2 \times 10^{-3}$ (dashes), divergence contribution for $\Delta\varphi = 0.5$ mrad (dots), combined contribution (solid curve).

The use of focusing and selection of a broader bandpass monochromator can be used to increase X-ray flux but at a cost of the loss of instrumental resolution. This loss of resolution should not be so large as to significantly broaden the peak widths of the samples under study and this therefore places a limit on the X-ray flux gains that can be achieved. We have investigated a series of samples which have been measured on station 9.1 and we conclude that an optimum optical arrangement would produce an X-ray beam with a bandpass of $\sim 2 \times 10^{-3}$ and with a divergence of about 0.5 mrad.

Focusing only affects the instrumental resolution in the plane of the focusing; therefore, in the perpendicular diffraction plane (*i.e.* horizontal plane if the focusing is in the vertical direction) there is no contribution to experimental resolution due to focusing. A test to show whether there is significant resolution broadening from the focusing is to determine whether diffraction peaks show an increase in width in the focusing plane relative to the perpendicular plane. As the instrumental broadening caused by focusing depends on the width of the X-ray fan collected, reducing the X-ray beam width using slits can reduce the focusing contribution, although at the cost of X-ray flux.

Fig. 2 shows the calculated d-space instrumental resolution ($\Delta d/d$) that would be obtained for an X-ray beam divergence of 0.5 mrad and an energy bandwidth ($\Delta E/E$) of 2×10^{-3}. The energy bandwidth contribution to instrumental resolution is only significant for low d-spacing reflections ($d < 1$ Å) while at high d-spacing the angular contribution dominates.

3. Beamline focusing optics

3.1. Requirements and limitations

With a divergent beam and small sample area, it is necessary to collimate the X-ray beam close to the sample in order to limit beam spread. In the case of a 70 µm pinhole and a beam of divergence 0.5 mrad, it is necessary to place the pinhole at $\sim$30 mm or less from the sample to prevent significant spread of the X-ray beam at the sample position. Our requirement is for beamline optics that produce a focused beam spot matched to the 70 µm pinhole placed just before the DAC. The optics should give a monochromatic beam with a bandpass of $\sim 2 \times 10^{-3}$ and energy of about 30 keV. The energy need not be continuously tunable, although it would be advantageous to be able to select higher energies for more absorbing samples, or to obtain a wider range of d-spacings, if required. We had two choices of location for the experiment, station 9.1 or station 9.5, also situated on the 5 T superconducting wavelength shifter but positioned 4 mrad from the centre of the horizontal radiation fan.

Station 9.1 is close to the source (15 m) but in the small experimental hutch only about 1 m is available for focusing. Station 9.5, although further from the source (30 m), has a larger experimental hutch with 4 m available for focusing. In both stations the optics could be placed in the white beam entering the hutch. Station 9.5 sees a single tangent point source from the superconducting wavelength shifter with magnetic field close to 5 T and therefore has a slightly harder X-ray energy spectrum than station 9.1, which sees two lower field tangent point sources. The flux density on station 9.5 is approximately a factor of four lower than that on station 9.1 because of the factor of two greater distance from the source. However, the requirement to limit beam divergence to less than 1 mrad allows a larger beam to be focused on station 9.5 owing to the longer available distance between focusing element and focus. On station 9.5 a 4 mm-wide beam could be focused with a 1 mrad divergence, while on station 9.1 a beam of only 1 mm could be focused with the same 1 mrad divergence.

The longer focusing distance available on station 9.5 makes focusing easier to implement as longer focal length optics require less strong focusing, and the extra space available around the experimental table offers the possibility of new dedicated layouts for high-pressure experiments.

3.2. Survey of possible X-ray optical systems

We considered a number of possibilities for selecting a monochromatic X-ray beam. A multilayer monochromator has a large bandpass ($\Delta E/E$ in excess of 10^{-2}) which leads to unacceptable loss of resolution. Perfect (unbent) crystal optics such as that used on station 9.1, on the other hand, have a narrow bandpass (10^{-4} or less) which does not give enhanced X-ray flux. A third option is to use bent crystal optics, which give a broadened bandpass.

For focusing the X-rays we also considered using mirrors or refractive lenses. Mirrors would need to operate at glancing incident angle to operate at this high energy; an incident angle of about 2 mrad would be required at 30 keV. For a 1 m-long mirror, this would limit the X-ray beam collected by the mirror to 2 mm. To obtain the short focal length with refractive lenses would require many stacked lenses but, as the off-axis X-rays suffer greater absorption, this limits the aperture that can be focused to less than 500 µm.

A simple solution is to use the monochromator crystal to focus the X-rays, requiring just a single optical element. This requires the monochromator to satisfy simultaneously the bandpass requirement and the focusing conditions. In order to focus, the crystal should be bent, but this bend can also be used to broaden the bandpass to the required level. For Laue monochromators, the crystal can be bent transversely to the focusing direction (sagittal bend) or parallel to the focusing direction (meridional bending). It is advantageous for the monochromator diffraction plane to be horizontal so that the focused monochromatic beam is horizontal. With a horizontal diffraction plane, a sagittally bent crystal focuses in the vertical direction and a meridionally bent crystal focuses in the horizontal direction.

3.3. Radiation characteristics

The requirement to limit the beam divergence to 0.5 mrad limits the fan of radiation that can be collected by the focusing element to 2 mm on station 9.5 where the focusing distance available is 4 m. There is a large fan of radiation available in the horizontal direction, but in the vertical direction synchrotron radiation is emitted into a narrow fan owing to the relativistic velocity of the electron beam source ($\gamma \simeq 4000$). Even so, at 30 m from the source the X-ray beam from a high-field insertion device is several millimetres high. Fig. 3 shows the calculated flux density profile at the proposed monochromator position at station 9.5. This shows that over an aperture of 2 mm (± 1 mm from the beam centre) the intensity drops only a few percent below the intensity at the beam centre. Given that the aperture must be limited to 2 mm, a vertically focusing device could be used with a negligible loss of intensity relative to horizontal focusing.

3.4. Bent crystal optics (Bragg or Laue sagittal focusing)

Bragg and Laue optics can both be bent for focusing purposes. A sagittally bent crystal in Bragg geometry (Sparks *et al.*, 1980) can be combined with a flat crystal to make a double-crystal monochromator capable of focusing a large aperture, but a narrow bandpass makes such a device unsuitable for this application. Single bent Bragg crystals can be used to focus meridionally in the Johann geometry but suffer from asymmetry in the reflectivity curve (Johann, 1931; Erola *et al.*, 1990). In contrast, the reflectivity curve of Laue optics conforms to an ideal top-hat shape and can give high peak reflectivity (Erola *et al.*, 1990; Zhong *et al.*, 2003). This reflectivity profile gives the highest integrated reflectivity for a given bandpass and therefore allows the X-ray flux to be maximized. Laue focusing has been demonstrated in meridional bending (Lienert *et al.*, 1998) and sagittal bending geometries (Zhong *et al.*, 2001*a*,*b*). Here, as X-rays are not required to make a low angle with the crystal surface, focusing can be achieved at high energies using a low-order wide-bandpass reflection. Another advantage of focusing in the Laue mode is that the bandwidth broadening can be tailored by choosing the crystal thickness. Taking into account these characteristics, we have developed a Laue sagittal focusing system for station 9.5.

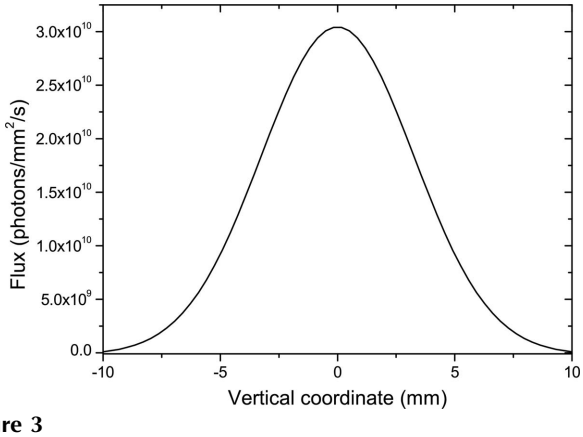

Figure 3
Calculated flux density profile as a function of vertical position about the beam centre at the monochromator location on station 9.5, 30 m from the source.

4. Optics of the Laue monochromator

4.1. Geometry of Laue focusing optics

The sagittal Laue geometry (Zhong *et al.*, 2001*a*,*b*) means that the focusing direction is perpendicular to the plane of diffraction of the monochromator. With a crystal bent in the sagittal direction the diffracting crystal planes for a symmetrical reflection remain parallel, and therefore symmetric reflections cannot be used for focusing. The diffracting planes for non-symmetric reflections do change orientation when the crystal is bent allowing these reflections to be used for focusing of the X-ray beam.

For simplicity, we use a horizontally deflecting single-crystal sagittally bent Laue monochromator to provide a monochromatic beam for the DAC experiment. In this arrangement the monochromatic beam is deflected from the incident white beam by an angle of 2θ and focusing takes place in the vertical direction. We are thus able to maintain the DAC and image plate in a horizontal plane, simplifying the experimental geometry. There is sufficient available vertical fan of radiation to gain significant benefit from the focusing.

4.2. Implementation of Laue focusing

The bender for the monochromator is a compact design with two lever arms holding the crystal. Manual adjustment is made to apply a curve of radius $\sim$1 m to the silicon wafer. To select energy, the bender is mounted on a motorized stage that rotates in the horizontal plane. The Laue crystals are made by cleaving commercially available silicon (100) wafers along (110) planes. Sagittal focusing requires an asymmetric diffraction geometry which can be achieved as the (111) planes are at an angle of 35.26° [$\sin^{-1}(1/3^{1/2})$] to the (110) cleavage planes. White-beam radiation strikes the (100) face of the oblong silicon crystal, which is arranged with its vertical edges parallel to (110). The geometry of the monochromator required to give the required energy of the (111) reflection is shown in Fig. 4.

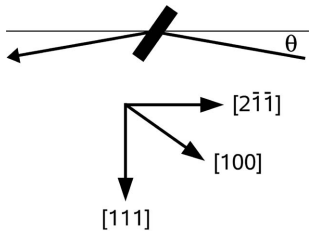

Figure 4
Geometry of the Laue monochromator (solid bar) viewed from above, showing unit-cell directions of the silicon crystal, and the (111) plane (thin solid line) from which X-rays are reflected. The Bragg angle (θ) gives the required energy of the (111) reflection. The angle between the [2$\bar{1}\bar{1}$] and [100] directions is 35.26°.

5. Experimental development

White radiation entering the hutch has longer wavelengths attenuated by a water-cooled aluminium absorber, reducing heat loading on the silicon monochromator. The shape of the beam on the monochromator is defined by a tungsten mask on the front face of the attenuator. The monochromator is operated in air; a lead block placed after the monochromator stops direct white beam. Lead shielding surrounding the monochromator reduces background scatter in the hutch to a minimum. The focused beam is directed through a 4 m-long evacuated beam tube. At the far end of this tube, the focused beam enters the atmosphere and is defined by a pinhole–collimator assembly. A platinum pinhole defines the beam size; a tungsten carbide collimator cuts scatter from the pinhole. Slits at the front end of the evacuated beam tube define the height of the monochromatic beam, and thus the vertical divergence after the pinhole.

The pinhole assembly, sample stage and detector (mar345 image plate) are located on a table which has horizontal translation perpendicular to the white beam direction and a vertical rotation axis allowing alignment of instrumentation with the monochromatic beam (Fig. 1*b*). To select the X-ray energy, the pinhole assembly is scanned horizontally as the monochromator is rotated. The absorption edge of a metal foil (usually indium) placed close to the monochromator is used to calibrate the energy of radiation. The indium *K*-edge gives λ = 0.44397 Å (27.93 keV). The height of the focused beam at the pinhole position measured by scanning a 50 µm slit vertically through the beam is about 85 µm (FWHM). The focus size calculated from the source size (450 µm) and the demagnification ratio of the optics (30 m from monochromator to source; 4 m from monochromator to focus) is ∼60 µm (4/30 × 450). When we deconvolute the effect of the 50 µm slit, we obtain a focus size of ∼67 µm, which compares favourably with the demagnified source size.

This indicates that the optics are effectively imaging the source (in the vertical direction) and introduce very little blurring. The energy bandwidth of the beam was measured by scanning the beam across the *K*-edge of an indium absorbing foil. The broadening of the sharp absorption edge indicated a bandwidth of $\Delta E/E \simeq 2.5 \times 10^{-3}$, close to our target figure. A motorized sample stage allows remotely controlled *x*, *y* and *z* translations, rotation about the vertical axis (ω), and a base translation which brings the rotation axis into the beam.

6. Experimental results from the station

6.1. Silicon

To compare the performance of stations 9.1 and 9.5, silicon powder (NIST 640b) held in adhesive tape has been measured on stations 9.1 (image plate) and 9.5 (mar345 detector). Integrated data from these measurements are shown in Fig. 5. Data from station 9.1 were collected with an exposure of 1800 s, and those from station 9.5 in 300 s. Although signal-to-noise ratios are similar, the intensity gain (∼×100) obtained from station 9.5 is obvious from this figure.

6.2. Hafnium tungstate

In this experiment a DAC was loaded with HfW_2O_8 (Evans *et al.*, 1996), without pressurization, and exposed for 120 s on station 9.5 using a pinhole size of 70 µm. The diffraction pattern integrated from the mar345 image-plate data (*Fit2d*; Hammersley *et al.*, 1996) is shown in Fig. 6, with well resolved diffraction peaks out to ∼25° 2θ ($d \simeq 1$ Å). Diffraction peaks have been individually fitted using split Pearson VII peak fitting in *TOPAS* (Bruker AXS, 2003) to obtain 2θ positions and FWHM errors. These fits have been used to calculate *d*-spacings and Δd (at FWHM) for each peak in the diffraction pattern. These data are plotted in Fig. 7 as $\Delta d/d$ against *d*, along with $\Delta d/d$ values calculated from a high-resolution powder diffractometer scan of silicon from station 9.1 (Bushnell-Wye & Cernik, 1992), from silicon diffraction recorded on station 9.1 using an image plate, and from silicon diffraction recorded on station 9.5 using the mar345 image plate. Here we can see that, as expected, the resolution of data

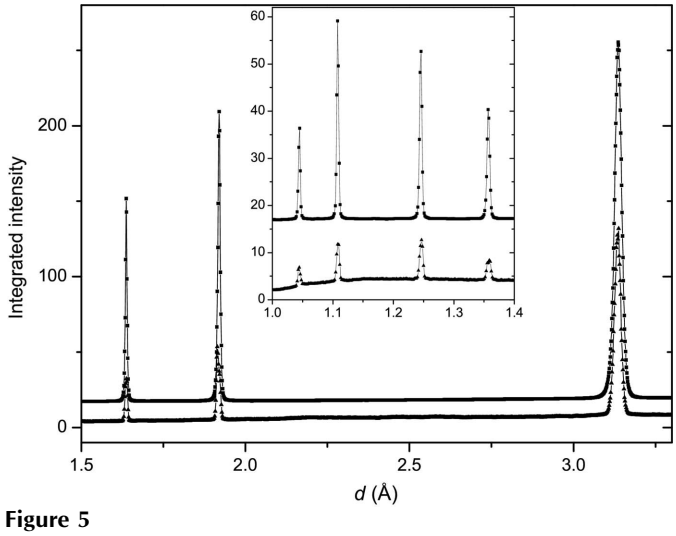

Figure 5
Integrated silicon powder diffraction patterns recorded on stations 9.1 (1800 s, image plate) and 9.5 (300 s, mar345 camera) using the arrangements shown in Fig. 1 and a pinhole size of 70 µm. The data from station 9.5 (squares, upper diffraction trace) have been divided by 7 and slightly offset. The intensity gain over station 9.1 (triangles, lower diffraction trace) is ∼100.

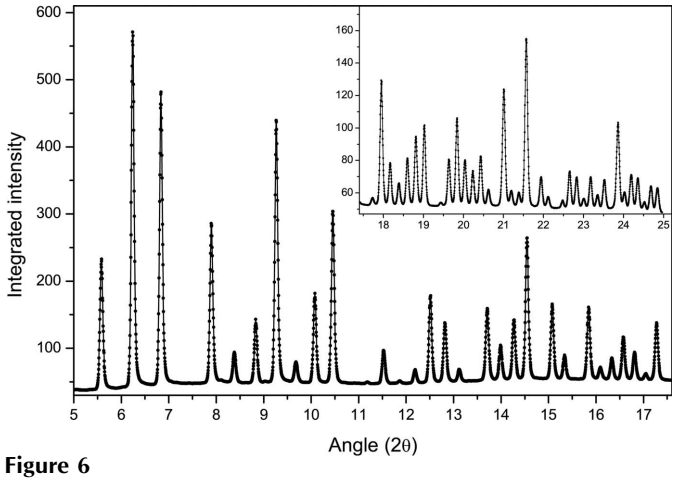

Figure 6
Diffraction pattern of HfW_2O_8 integrated using *Fit2d* from mar345 image-plate data obtained on station 9.5. The sample, held in a DAC at ambient pressure, was exposed for 120 s to obtain the image from which this pattern was integrated.

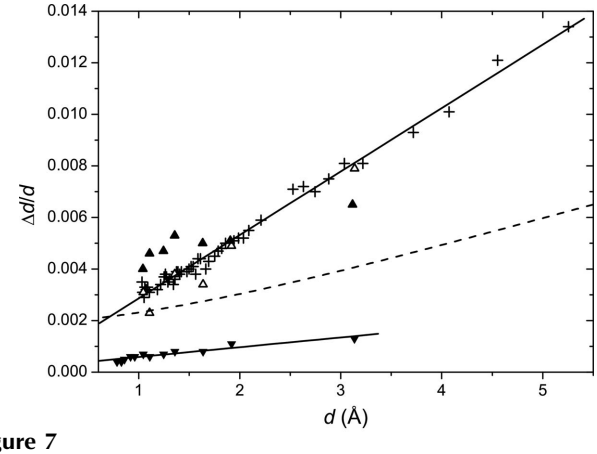

Figure 7
Comparison of resolution ($\Delta d/d$ against d) between silicon diffraction from the station 9.1 diffractometer (filled inverted triangles), station 9.1 image plate (filled triangles) and station 9.5 mar345 image plate (open triangles), and from HfW_2O_8, station 9.5 mar345 image plate (plus signs). The dashed curve shows the calculated combined bandwidth and divergence contribution to resolution. Solid lines are least-squares fits to HfW_2O_8 and silicon data.

collected on station 9.1 with the diffractometer is clearly higher than that integrated from the image plate on the same station, even though the same monochromator is used to produce monochromatic X-rays for these two experiments. The resolution of data from the high-pressure experimental set-up on stations 9.1 and 9.5 are comparable, indicating that resolution here is defined by image-plate resolution and not by monochromator resolution.

7. Summary

With the flux intensity achieved by the Laue monochromator, we have been able to insert a pinhole of diameter $\sim$25 µm, still allowing measurements on samples held in DACs at up to 70 GPa to be made in a reasonable time. Short exposure and data read-out times thus allow experiments new to the SRS. We have used this project to develop a new X-ray station at relatively modest cost, showing the effectiveness of the Laue focusing monochromator for producing X-rays for diffraction experiments requiring medium resolution. This optical and beamline configuration could be installed easily on a third-generation synchrotron, where bending magnets have X-ray characteristics comparable with the beamline 9 wiggler on the SRS at $\sim$30 keV. The large vertical fan of a third-generation bending magnet, and the geometry of the monochromatic beam from the Laue monochromator, which takes the X-ray beam away from the shield wall, would allow construction of a new beamline at modest cost.

We wish to thank Don Abram, Rod Birchall, Norman Brookfield, Ian Burrows, Graeme Donaldson, John Flaherty, Barry Hammond, Malcolm Miller, Mike Miller, Alfie Neild, William Owen and Frances Quinn for their contributions to the success of this project. We thank Michael Henderson for creating the opportunity for development of this beamline.

References

Bruker AXS (2003). *TOPAS User's Manual. General Profile and Structure Analysis Software for Powder Diffraction Data.* Version 2.1. Bruker AXS, Karlsruhe, Germany.
Bushnell-Wye, G. & Cernik, R. J. (1992). *Rev. Sci. Instrum.* **63**, 999–1001.
Erola, E., Eteläniemi, V., Suortti, P., Pattison, P. & Thomlinson, W. (1990). *J. Appl. Cryst.* **23**, 35–42.
Evans, J. S. O., Mary, T. A., Vogt, T., Subramanian, M. A. & Sleight, A. W. (1996). *Chem. Mater.* **8**, 2809–2823.
Hammersley, A. P., Svensson, S. O., Hanfland, M., Fitch, A. N. & Hausermann, D. (1996). *High Press. Res.* **14**, 235–248.
Hemley, R. J., Mao, H.-K. & Struzhkin, V. V. (2005). *J. Synchrotron Rad.* **12**, 135–154.
Johann, H. H. (1931). *Z. Phys.* **69**, 185–206.
Lienert, U., Schulze, C., Honkimäki, V., Tschentscher, Th., Garbe, S., Hignette, O., Horsewell, A., Lingham, M., Poulsen, H. F., Thomsen, N. B. & Ziegler, E. (1998). *J. Synchrotron Rad.* **5**, 226–231.
McMahon, M. I. (2004). In *High-Pressure Crystallography*, *NATO Science Series*, edited by A. Katrusiak and P. McMillan. Dordrecht: Kluwer.
Nelmes, R. J., Hatton, P. D., McMahon, M. I., Pilz, R. O., Crain, J., Cernik, R. J. & Bushnell-Wye, G. (1992). *Rev. Sci. Instrum.* **63**, 1039–1042.
Shimomura, O., Takemura, K., Fujihisa, H., Fujii, Y., Ohishi, Y., Kikegawa, T., Amemiya, Y. & Matsushita, T. (1992). *Rev. Sci. Instrum.* **63**, 967–973.
Sparks, C. J., Borie, B. S. & Hastings, J. B. (1980). *Nucl. Instrum. Methods*, **172**, 237–242.
Warren, B. E. & Averbach, B. L. (1950). *J. Appl. Phys.* **21**, 595–599.
Zhong, Z., Kao, C. C., Siddons, D. P. & Hastings, J. B. (2001*a*). *J. Appl. Cryst.* **34**, 504–509.
Zhong, Z., Kao, C. C., Siddons, D. P. & Hastings, J. B. (2001*b*). *J. Appl. Cryst.* **34**, 646–653.
Zhong, Z., Kao, C. C., Siddons, D. P., Zhong, H. & Hastings, J. B. (2003). *Acta Cryst.* A**59**, 1–6.